Applied Physics B (2018) 124:87
https://doi.org/10.1007/s00340-018-6960-7

Applied Physics B
Lasers and Optics

Dual-wavelength operation of a diode-pumped Nd:YVO_4 laser at the 1064.1 & 1073.1 nm and 1064.1 & 1085.3 nm wavelength pairs

Tanant Waritanant[1] · **Arkady Major**[1]

Received: 7 February 2018 / Accepted: 21 April 2018 / Published online: 2 May 2018

Abstract
Two dual-wavelength operation regimes of a diode-pumped Nd:YVO_4 laser were demonstrated at 1064.1 & 1073.1 and 1064.1 & 1085.3 nm with two intracavity birefringent plates. The output power ratio of the dual-wavelength output could be freely adjusted. The highest total output power was 1.44 W under the dual-wavelength condition with 1:1 power ratio for both wavelength pairs. The slope efficiency was more than 16% and optical-to-optical efficiency more than 13% with respect to the absorbed pump power.

1 Introduction

Dual-wavelength lasers or lasers with simultaneous output at two different frequencies have been at a focus of several recent studies due to multiple promising applications in biomedicine such as blood analysis, DNA sequencing, flow cytometry, microscopy, and optogenetics [1–7]. With appropriate wavelength spacing of a dual-wavelength output it can be also converted to a coherent terahertz (THz) radiation through difference frequency generation (DFG) [8]. THz radiation falls into the very attractive spectral range with unique properties and promising potential for THz imaging, sensing, and THz spectroscopy applications [9–11].

There are multiple methods to achieve dual-wavelength operation, all of which are based on the balanced round-trip gains at the two wavelengths. Dual-wavelength generation in solid-state lasers can be separated into the three main categories. The first method to obtain dual-wavelength operation is to have two crystals with similar emission cross-sections to have comparable gain at different wavelengths. This method can also be extended to incorporate hybrid laser gain medium [12] or gain medium with multiple dopants [13]. The second method utilized the fact that in some uniaxial or biaxial crystals, the emission peaks for horizontal and vertical polarizations occur at different wavelengths [14]. Therefore, by choosing a proper direction of crystal cut, orthogonally-polarized laser operations can take place [15, 16]. These first two approaches in obtaining a dual-wavelength operation rely on a very strict balance of round-trip gains which is easily disturbed by the cavity conditions such as thermal lensing or fluctuation in the pump power. This can lead to poor control of power ratio between the two oscillating wavelengths. The last type of dual-wavelength generation is obtained by inserting an extra loss element inside the laser cavity. This is generally done using a specific coating of the output coupler (OC) to intentionally have high reflectivity at low gain wavelength of the laser crystal and low reflectivity at high gain wavelength [1, 17]. However, a specific coating of the OC also means that the dual-wavelength laser will again operate on a strict condition of roundtrip-gain equalization and will only work at a certain power level. To allow for more flexibility in the setup, wavelength tunable loss elements such as etalons [18], Fabry–Perot filters [19], or birefringent filters (BRF) [20] are better suited for dual-wavelength generation. The latter approach is a particularly simple one because of ease of use and manufacturing. For example, in case of broadband gain media (such as Ti:sapphire, Alexandrite and Yb:KGW) that are usually used to produce ultrashort pulses [21–28] for various applications [29–35], the BRF technique was recently successfully used to achieve dual-wavelength operation [36–40]. At the same time, the sharp transition lines of the Nd-ion-doped crystalline gain media [41] in combination with BRF can also be used for multiwavelength operation [42, 43].

Among the gain media for diode-pumped solid-state lasers, the crystals of Nd:vanadate (Nd:YVO_4) stand out as suitable

✉ Arkady Major
a.major@umanitoba.ca

[1] Department of Electrical and Computer Engineering, University of Manitoba, Winnipeg, Canada

candidates for compact and efficient diode-pumped lasers in the medium power range (< 10W) applications since they provide many advantages such as high absorption and emission cross sections, strongly polarized emission, and reasonable thermal conductivity. Considering the observed emission lines at 1064, 1073, and 1085 nm [42], the possible dual-wavelength pairs that Nd:YVO_4 can offer are 1064 & 1073, 1064 & 1085, and 1073 & 1085 nm all of which are spaced with a few THz frequency offset. Moreover, the 1073 nm emission line has not been reported in dual-wavelength operation from the Nd:YVO_4 crystal even though its stimulated emission cross-section is comparable to the one at 1085 nm. This is possibly due to its proximity to the strongest 1064 nm emission line. In this work, we demonstrated the ability to achieve gain balancing for two of the mentioned wavelength pairs through the use of two intracavity BRF plates.

2 Principle of operation

In our case two quartz BRFs with in-plane optical axes, as seen in Fig. 1 (only one BRF is shown), were placed into the laser cavity at the Brewster's angle (θ_B) and introduced tunable wavelength-dependent loss through rotation of the plates around their surface normals [20].

Regarding the dual-wavelength operation itself, in order for two wavelengths to 'start' oscillating at the same time, it is required that the threshold pump power P_{th} levels for both wavelengths, e.g. 1064 and 1073 nm, were the same [13, 44]. From the threshold pump power expression given in [45], the condition for the same threshold pump power for the two laser wavelengths becomes,

$$\frac{L_{1064} - \ln\left(1 - T_{oc}\right)}{\sigma_{1064}\eta_{1064}} = \frac{L_{1073} - \ln\left(1 - T_{oc}\right)}{\sigma_{1073}\eta_{1073}}, \tag{1}$$

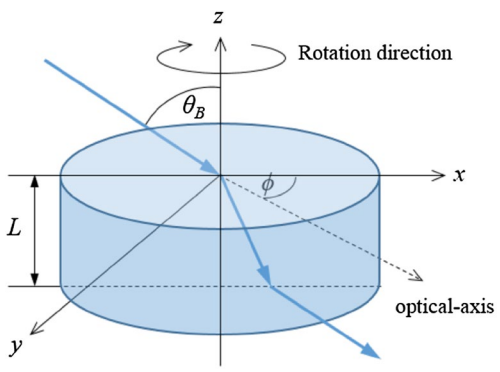

Fig. 1 A drawing of the birefringent plate, angles, and the corresponding notations

where L is the round trip intracavity loss, T_{oc} is the transmission of the output coupler, σ is the emission cross-section at the laser wavelength, and η is the quantum efficiency. This condition is possible even with a single intracavity BRF plate as demonstrated in [42], where the transmission at 1064 nm at a certain angle of a BRF exactly equals the required transmission at which the two wavelengths experience the same P_{th}. However, the 'first' problem is that the angular tolerance of such a condition is very small (~0.1°), making it hard to perfectly achieve and control in practice, thus leading to unstable power ratio at the two wavelengths over a long period of time.

It is also worth noting that equal threshold condition described by Eq. (1) does not automatically translate into the equal output power ratio between the oscillating wavelengths *above the threshold* which is the 'second' problem. Unlike other methods of dual-wavelength generation, the benefit of using BRF plates is that they enable not only to select the correct threshold condition via changes in the L_{1064} and L_{1073} losses (i.e. BRF introduced losses) but also to reach 50% power ratio at all power levels which is generally much more complicated [19].

To illustrate the problem of gain balancing at power levels at and beyond P_{th}, we recall that the laser output power (P_{out}) is described by [46]

$$P_{out} = \frac{-\ln(1 - T_{oc})}{-\ln(1 - T_{oc}) + L_\lambda}\frac{v_L}{v_p}\left(P_{abs} - P_{th,\lambda}\right), \tag{2}$$

where λ refers to the laser wavelength, v_L is the laser frequency, v_p is the pump frequency, and P_{abs} is the absorbed pump power. This equation also shows the expanded form of slope efficiency (η_s) of a given laser system ($P_{out} = \eta_s (P_{abs} - P_{th,\lambda})$). With this in mind, let us consider a scenario when there is no intracavity BRF plate in the laser cavity. In such a case the intracavity losses are the same at both wavelengths ($L_{1064} = L_{1073}$) whereas Eq. (1) dictates that $P_{th,1064} < P_{th,1073}$ because of the difference between the emission cross-sections ($\sigma_{1064} > \sigma_{1073}$). This laser operation is schematically drawn in Fig. 2a. As P_{abs} increases, the output power (P_{out}) at 1064 nm also increases with the slope efficiency ($\eta_{s,1064}$) described by the Eq. (2) with no dual-wavelength operation. The emission at 1073 nm will not be observed due to a higher threshold.

In the next step (Fig. 2b), we introduced an additional intracavity loss from a single BRF plate which helps to fulfill the exact condition described by Eq. (1) ($L_{BRF,1064} > L_{BRF,1073}$) and leads to $P_{abs} = P'_{th,1064} = P'_{th,1073}$. This point is shown as the starting point (white circle) in Fig. 2b. Equation (2) shows, however, that the higher loss introduced at 1064 nm (high $L_{BRF,1064}$ and, ultimately, high L_{1064}) to achieve the same threshold pump power will result in the lower slope efficiency ($\eta'_{s,1064}$) at this wavelength

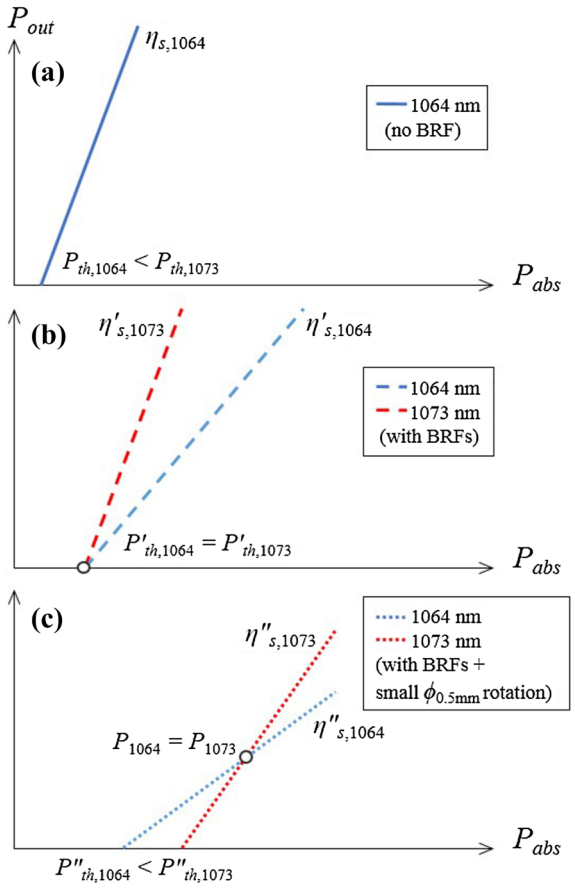

Fig. 2 Simple illustrations of the change in output power versus the absorbed pump power of single- and dual-wavelength lasers for various conditions involving birefringent filter tuning

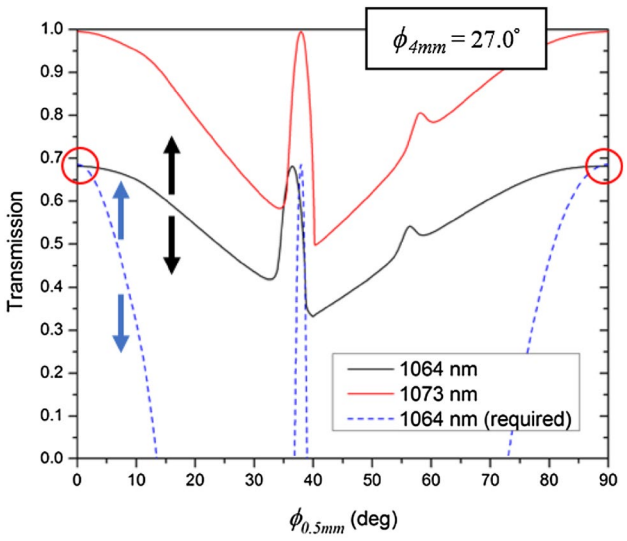

Fig. 3 Transmissions of the 1064 and 1073 nm wavelengths through both 4-mm-thick and 0.5-mm-thick BRF plates as well as the required transmission at 1064 nm (blue dashed curve) for dual-wavelength operation. The crossing points of the 1064 nm (black) and the required (blue dashed) curves indicate the condition of equal thresholds for 1064 and 1073 nm wavelengths. The fixed angle of the 4-mm-thick BRF plate is indicated in the graph as $\phi_{4\,mm}$

than at 1073 nm ($\eta'_{s,1073}$). Therefore, above the threshold at $P_{abs} > P'_{th,1064} = P'_{th,1073}$, the levels of P_{out} at the two wavelengths will start to diverge. As shown by the two lines in Fig. 2b, this means that the dual-wavelength operation with equal power ratio for the oscillating wavelengths can only be achieved at a certain level of P_{abs}. This describes the second problem mentioned earlier.

To solve both of these problems, an extra loss element can be used with lower angular sensitivity, which can be found in thin BRF plates featuring broad transmission linewidths [20]. The effect of having two BRFs with different thicknesses in the cavity is shown in Fig. 2c. The introduced extra loss from a thin BRF reduces the slopes and increases the thresholds for both wavelengths. Most importantly, with proper alignment of a thin BRF, it can shift the threshold of 1073 nm to a higher value of the absorbed pump power than that for 1064 nm. Therefore, by breaking the condition of equal thresholds and due to the different slopes of the two wavelengths, one can achieve equal power dual-wavelength oscillation well above the threshold. As a side effect, at each pump power level this regime would require a slightly different amount of the introduced intracavity loss which can be conveniently found by rotation of a thin BRF.

For example, let us consider the transmissions at 1064 and 1073 nm wavelengths with the 4-mm-thick intracavity BRF plate kept at a constant angle of rotation of 27.0° ($\phi_{4\,mm} = 27.0°$) while the second, 0.5-mm-thick, BRF plate is rotated from $\phi_{0.5\,mm} = 0°$ to $\phi_{0.5\,mm} = 90°$. The choice of the plate thicknesses was based on our previous discrete wavelength tuning work in Nd:YVO_4 lasers [42, 43]. The transmission through both BRF plates is shown in Fig. 3 which was obtained from Jones matrix calculations [20]. At $\phi_{0.5\,mm} = 0°$ point, there is no loss introduced by the BRF plate at 1073 nm ($L_{BRF,1073} = 0$) while $L_{BRF,1064} = 0.32$. The required transmission at 1064 nm (blue dashed line) in Fig. 3 is the transmission level at 1064 nm that is required to fulfill the condition given by Eq. (1). The overlapped sections (in red circles) of the 1064 nm transmission and the required transmission at 1064 nm represent $P_{th,1073} \approx P_{th,1064}$ condition and will have the largest angular tolerance when the slopes of both lines are at the minimum. As can be seen, this occurs at 0° and 90° of rotation angles of the 0.5-mm-thick BRF plate and can be compared to the $\phi_{0.5\,mm} \approx 38°$ case which has a very tight angular tolerance (~0.1°). Fine tuning of the starting condition can then be accomplished by rotating the thin BRF away from 0° and 90°. Therefore, two birefringent filters allow for more precise control over the conditions of the two oscillating wavelengths thus solving the 'first' problem and allowing for higher long-term stability.

Similar to the drawing in Fig. 2b, the discussed parameters result in a dual-wavelength operation only around the threshold pump power which is not practical.

The 'second' problem of how to maintain the equal power ratio far above the threshold ($P_{\text{out},1064} = P_{\text{out},1073}$ at $P_{\text{abs}} >> P_{\text{th}}$) can also be solved by the rotation of the thin BRF further away from the starting positions at either $\phi_{0.5\text{ mm}} = 0°$ or $\phi_{0.5\text{ mm}} = 90°$. Qualitatively, since by rotating the 0.5-mm-thick BRF plate we are simultaneously reducing transmission at both wavelengths (i.e. increasing losses by $\Delta L_{\text{BRF},1064} \approx \Delta L_{\text{BRF},1073} \approx \Delta L_{\text{BRF}}$ as seen in Fig. 3), the Eq. (1) tells us that this causes the $P''_{\text{th},1073}$ to be higher than $P''_{\text{th},1064}$. This happens because the right side of Eq. (1) is much more sensitive to the change of intracavity loss which was previously kept at the minimum value. Equation (2) also makes sure that the resulting slope $\eta''_{\text{s},1064}$ after the rotation of the thin BRF (with $\Delta L_{\text{BRF},1064} \approx \Delta L_{\text{BRF},1073} \approx \Delta L_{\text{BRF}}$) is still lower than $\eta''_{\text{s},1073}$ due to the larger total intracavity loss ($L_{1064} = L_{\text{in}} + L_{\text{BRF},1064} + \Delta L_{\text{BRF}} > L_{1073} = L_{\text{in}} + \Delta L_{\text{BRF}}$).

The two restrictions set by the Eqs. (1) and (2) above mean that at all pump power P_{abs} levels beyond the starting point at threshold ($P_{\text{abs}} > P'_{\text{th},1064} = P'_{\text{th},1073}$), it would be always possible to find a $P_{\text{out},1064} = P_{\text{out},1073}$ situation since there will always be an intersection between the two output power lines as shown in Fig. 2c. This can be ensured providing that the introduced ΔL_{BRF} intracavity loss by rotation of the thin BRF plate shifts the threshold condition away from the starting point. This also means that for a specific intracavity loss introduced by the two BRFs it would be possible to find the equal power dual-wavelength regime simply by adjusting the pump power level rather than the loss. Therefore, equal power regime can be stabilized either by the proper level of loss or pump power.

Therefore, two birefringent filters allow for a more precise control over the initial conditions ($P'_{\text{th},1064} = P'_{\text{th},1073}$) of the two oscillating wavelengths thus allowing for a higher long-term stability as well as helping in maintaining the equal power ratio at subsequent output power levels.

As a side note, the overlapping of the transmission at 1064 nm and the required transmission at the starting point as shown in Fig. 3 can be ensured by two factors. First, by changing between the different values of $\phi_{4\text{ mm}}$ (for example, to other values besides 27.0°), the starting points of 1064 nm transmission can be discretely selected (black arrows in Fig. 3) while keeping the transmission at 1073 nm still at the maximum. Second, it is worth noting that aside from changing the $\phi_{4\text{ mm}}$ rotation angle, the insertion angle can be also purposefully chosen slightly off from the Brewster's angle, therefore, increasing L_{in} and changing the level of the required transmission at 1064 nm (blue arrows). This should be used with caution because any deviation from the Brewster's angle also affects losses at 1073 nm. With these two factors chosen carefully, the starting points displayed in Fig. 3 can be easily achieved. Finally, similar conditions can also be found in the case of dual-wavelength operation between the 1064 and 1085 nm.

3 Experimental details

A 5 mirror-cavity shown in Fig. 4 was used in the experiments with cavity lengths adjusted to accommodate the thermal lensing effect of about 160 mm [47]. The laser used a 20-mm-long, 1.5% doped crystal of an a-cut Nd:YVO_4. The crystal was pumped by up to 16.7 W of pump power at 914 nm from a fiber-coupled laser diode. This low quantum defect pump wavelength was chosen to minimize the effect of thermal lensing [48] and maximize laser efficiency [49–52]. The pump spot size diameter in the crystal was 550 µm. About 67% of the incident pump power was absorbed by the crystal. Two birefringent quartz filter plates, the 4 and 0.5-mm-thick, were used at the Brewster's angle in the laser cavity.

The 4-mm-thick birefringent filter plate was inserted into the cavity first and rotated until the 1073 nm (or 1085 nm) laser output was observed. This birefringent plate ensured that the 1064 nm line fell into the low transmission band of the filter. The second plate with 0.5 mm thickness was then inserted and adjusted until both wavelengths were present. Further fine optimization of rotation angles of both plates was necessary to achieve the highest output power. Among the multiple OCs available, the one with the 2.1% transmission in the 1040–1090 nm range was found to provide the highest output power in dual-wavelength operation.

4 Results and discussions

Dual wavelength oscillation was maintained within the range of 3–5 degrees of rotation of $\phi_{0.5\text{ mm}}$. At 11.2 W of absorbed pump power (16.7 W of incident pump power), the dual-wavelength operation with > 1 W of output power was observed at the 1064.1 & 1073.1 nm and 1064.1 & 1085.3 nm wavelength pairs after carefully adjusting of the

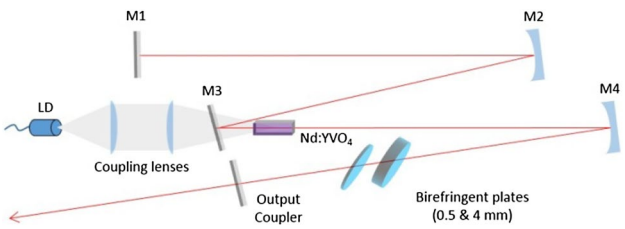

Fig. 4 Experimental setup for dual-wavelength operation

BRFs. The laser output power with 1:1 power ratio at every pump power level is presented in Fig. 5.

The maximum output power when each wavelength had a similar spectral intensity (1:1 power ratio) was 1.44 W in case of 1064 & 1073 nm operation. The slope efficiency was 16.53%. The output power reached 1.46 W in case of 1064.1 & 1085.3 nm dual-wavelength operation with the slope efficiency of 16.2%. Figures 6 and 7 show the output spectra for 1064.1 & 1073.1 nm and 1064.1 & 1085.3 nm operations, respectively. As expected, power ratio could be adjusted either by the rotation of the BRFs or pump power level.

Although the power ratio of the dual-wavelength output was still sensitive to the change in the pump power level of the laser and specific power ratio could only be maintained within a limited range of output power without the change in cavity parameters, it could be adjusted back to 1:1 throughout all of the output power levels by rotating the 0.5-mm-thick birefringent plate. The long-term stability of the average laser output power at the highest power level was better than 1% over 2 h with the fluctuation in the spectral power ratio of 2.14% as was obtained from the optical spectrum analyzer data. This measurement started from 1:1 power ratio and the maximum deviation of spectral intensity at 1073 nm over 1064 nm was recorded ($\Delta I_{1073}/I_{1064}$). In both dual-wavelength regimes the linewidths of each wavelength were ~0.1 nm and were limited by the resolution of the available spectrometer. When the 0.5-mm-thick birefringent filter plate was rotated until the laser was operating at a single laser wavelength again, the output powers were increased to 4.61 W, 3.83 W and 3.74 W for 1064.1, 1073.1, and 1085.3 nm wavelengths, respectively.

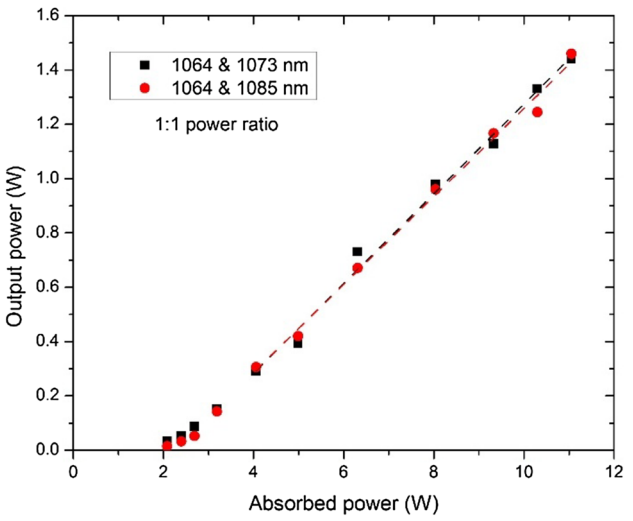

Fig. 5 Dual-wavelength output power at 1:1 power ratio versus absorbed pump power

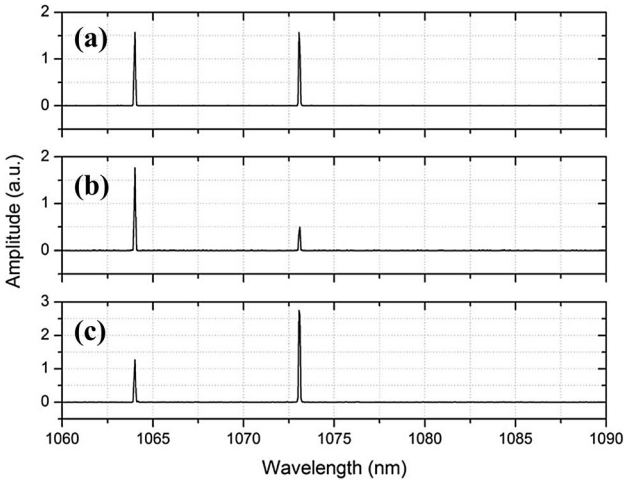

Fig. 6 Dual-wavelength operation spectra at 1064.1 and 1073.1 nm. **a**–**c** show the change in power ratio between the two output wavelengths by adjusting the rotation angle of the 0.5-mm-thick BRF plate

To compare the results achieved in this work, Table 1 shows a summary of the results of dual-wavelength Nd-doped lasers operating on the similar laser transitions.

As can be seen from Table 1, our result is the first dual-wavelength operation with two wavelength pairs at 1064 & 1073 nm and 1064 & 1085 nm achieved with the same laser setup without the need to replace any optical elements. The highest optical-to-optical efficiencies with controllable spectral power ratio were also demonstrated for both wavelength pairs which is desirable for the generation of THz radiation. At the same time, we have also achieved the highest output power in dual-wavelength regime. We believe that the output power can be scaled even further by

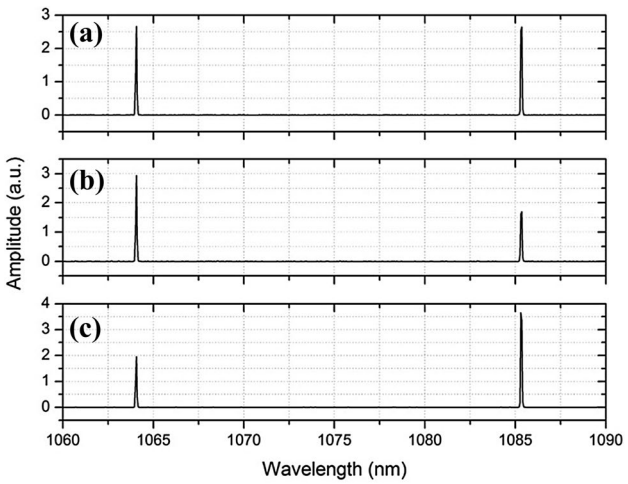

Fig. 7 Dual-wavelength operation spectra at 1064.1 and 1085.3 nm. **a**–**c** show the change in power ratio between the two output wavelengths by adjusting the rotation angle of the 0.5-mm-thick BRF plate

Table 1 Performance results of dual-wavelength Nd-doped lasers

Crystal	Wavelength pair (nm)	FrEq. difference (THz)	Method	Tunable power ratio demonstrated	P_{out} (W) at 1:1 power ratio	Opt-to-opt efficiency (%) at 1:1 power ratio	References
Nd:$LuVO_4$	1086/1089	0.7	2 polarizations	No	0.74	17.5	[15]
Nd:YVO_4	1066/1083,1085,1088	5.6	Etalon	No	-	8	[18]
Nd:YVO_4	1064/1085	5.57	Specific OC coating	No	N/A	N/A	[1]
Nd:LYSO	1075/1079	1.06	Specific OC coating	No	0.7	27.7	[17]
Nd:YAG	1116/1123	1.86	Etalon	No	-	9.2	[53]
Nd:YAG	1064/1073	2.4	Fabry–Perot filter	Yes	0.581	10.9	[54]
Nd:YVO_4	1064/1085	5.6	Fabry–Perot filter	Yes	0.156	1.38	[19]
Nd:YVO_4	1064/1073	2.39	2 BRFs	Yes	1.44	13.0	This work
	1064/1085	5.62	2 BRFs	Yes	1.46	13.2	

more careful optimization of BRF thicknesses and owing to the reduced thermal lensing offered by the low quantum defect pumping at 914 nm. The dual-wavelength operation at 1073 & 1085 nm was not observed in the experiment. Most likely this was caused by the close proximity of the strong 1064 nm line which made it difficult to suppress by the currently available combination of the BRF plates.

5 Conclusions

In conclusion, we have presented a method and explanation on how multiple BRFs can be used to achieve the power ratio tunable dual-wavelength operation of a Nd:YVO_4 laser. To the best of our knowledge, the results shown in this work were the first demonstration of the dual-wavelength Nd:YVO_4 laser operating at the 1064.1 & 1073.1 nm and 1064.1 & 1085.3 nm wavelength pairs with adjustable output power ratios and high output power stability. Both dual-wavelength pairs could be obtained with one setup with minor adjustments to the BRFs. The observed dual-wavelength output features > 1.4 W of output power and is very promising for applications in THz generation because the frequency difference of the oscillating wavelengths corresponds to the desirable range of THz radiation (1–10 THz). The high output power and efficiency of this method could lead to an efficient source of THz radiation. Finally, it is worth mentioning that multiple BRF plates can also be used to generate a more complex transmission shape and ultimately to balance the gain for more than one pair of wavelengths at a time.

This can lead to even tri-wavelength or multiwavelength operation [39] which is much harder to achieve with other tuning methods.

Acknowledgements The authors would like to acknowledge funding of this project provided by the Natural Sciences and Engineering Research Council of Canada, and the University of Manitoba.

References

1. G. Shayeganrad, L. Mashhadi, Appl. Phys. B **111**, 189 (2013)
2. J. Wang, Y. Wang, B. Li, D. Feng, J. Lu, Q. Luo, P. Li, Opt. Lett. **38**, 3690 (2013)
3. C.W. Pirnstill, B.H. Malik, V.C. Gresham, G. L. Cote Diabetes Technol. Ther. **14**, 819 (2012)
4. H.M. Shapiro, *Practical flow cytometry* (Wiley, Liss, 2003)
5. M.R. Jafarfard, S. Moon, B. Tayebi, D.Y. Kim, Opt. Lett. **39**, 2908 (2014)
6. M. Prigge, F. Schneider, S.P. Tsunoda, C. Shilyansky, J. Wietek, K. Deisseroth, P. Hegemann, J. Biol. Chem. **287**, 31804 (2012)
7. P. Hering, J.P. Lay, S. Stry, *Laser in environmental and life sciences: modern analytical method* (Springer, Heidelberg, 2003)
8. M. Scheller, J.M. Yarborough, J.V. Moloney, M. Fallahi, M. Koch, S.W. Koch, Opt. Express **18**, 27112 (2010)
9. J.F. Federici, B. Schulkin, F. Huang, D. Gary, R. Barat, F. Oliveira, D. Zimdars, Semicond. Sci. Technol. **20**, S266 (2005)
10. J.B. Baxter, G.W. Guglietta, Anal. Chem. **83**, 4342 (2011)
11. C.B. Reid, E. Pickwell-MacPherson, J.G. Laufer, A.P. Gibson, J.C. Hebden, V.P. Wallace, Phys. Med. Biol. **55**, 4825 (2010)
12. A.J. Singh, S.K. Sharma, P.K. Mukhopadhyay, S.M. Oak, Pramana J. Phys. **75**, 929 (2010)
13. B.M. Walsh, Laser Phys. **20**, 622 (2010)
14. H. Zhao, A. Major, Opt. Express **22**, 26651 (2014)
15. Y.P. Huang, C.Y. Cho, Y.J. Huang, Y.F. Chen, Opt. Express **20**, 2107 (2012)
16. H. Zhao, A. Major, Appl. Phys. B **122**, 163 (2016)
17. L. Chen, X. Xu, Z. Wang, D. Li, H. Yu, J. Xu, S. Zhuang, L. Guo, Y. Zhao, X. Xu, Chin. Opt. Lett. **9**, 071403 (2011)
18. G. Shayeganrad, Y. Huang, L. Mashhadi, Appl. Phys. B **108**, 67 (2012)
19. X. Wang, Z. Wang, Y. Bu, L. Chen, G. Cai, W. Huang, Z. Cai, N. Chen, Appl. Opt. **55**, 879 (2016)
20. K. Naganuma, G. Lenz, E.P. Ippen, IEEE J. Quantum Electron. **28**, 2142 (1992)

21. K. Lamb, D.E. Spence, J. Hong, C. Yelland, W. Sibbett, Opt. Lett. **19**, 1864 (1994)
22. S. Ghanbari, R. Akbari, A. Major, Opt. Express **24**, 14836 (2016)
23. A. Major, L. Giniunas, N. Langford, A.I. Ferguson, D. Burns, E. Bente, R. Danielius, J. Mod. Opt. **49**, 787 (2002)
24. R. Akbari, K.A. Fedorova, E.U. Rafailov, A. Major, Appl. Phys. B **123**, 123 (2017)
25. H. Zhao, A. Major, Opt. Express **22**, 30425 (2014)
26. R. Akbari, H. Zhao, K.A. Fedorova, E.U. Rafailov, A. Major, Opt. Lett. **41**, 3771 (2016)
27. A. Major, R. Cisek, V. Barzda, Proc. SPIE **6108**, 61080Y (2006)
28. S. Manjooran, A. Major, in *Conference on Lasers and Electro-Optics* (OSA, 2016), p. JTu5A.82
29. D. Sandkuijl, R. Cisek, A. Major, V. Barzda, Biomed. Opt. Express **1**, 895 (2010)
30. I.P. Nikolakakos, A. Major, J.S. Aitchison, P.W.E. Smith, IEEE J. Sel. Top. Quantum Electron. **10**, 1164 (2004)
31. A. Major, F. Yoshino, J.S. Aitchison, P.W.E. Smith, E. Sorokin, I.T. Sorokina, Appl. Phys. Lett. **85**, 4606 (2004)
32. H. Zhao, I.T. Lima Jr., A. Major, Laser Phys. **20**, 1404 (2010)
33. I.T. Lima, V. Kultavewuti, A. Major, Laser Phys. **20**, 270 (2010)
34. R. Akbari, A. Major, Laser Phys. **23**, 035401 (2013)
35. S. Manjooran, H. Zhao, I.T. Lima, A. Major, Laser Phys. **22**, 1325 (2012)
36. R. Akbari, H. Zhao, A. Major, Opt. Lett. **41**, 1601 (2016)
37. C.G. Treviño-Palacios, O.J. Zapata-Nava, E.V. Mejía-Uriarte, N. Qureshi, G. Paz-Martínez, O. Kolokolstev, J. Eur. Opt. Soc. **8**, 1 (2013)
38. S. Ghanbari, A. Major, Laser Phys. Lett. **14**, 105001 (2017)
39. U. Demirbas, R. Uecker, J.G. Fujimoto, A. Leitenstorfer, Opt. Express **25**, 2594 (2017)
40. S. Manjooran, P. Loiko, A. Major, Appl. Phys. B **124**, 13 (2018)
41. R. Moncorge, B. Chambon, J.Y. Rivore, N. Garnier, E. Descroix, P. Laporte, H. Guillet, S. Roy, J. Mareschal, D. Pelenc, J. Doury, P. Farge, Opt. Mater. **8**, 109 (1997)
42. T. Waritanant, A. Major, Opt. Lett. **42**, 1149 (2017)
43. T. Waritanant, A. Major, Opt. Lett. **42**, 3331 (2017)
44. Y. Chen, Appl. Phys. B **70**, 475 (2000)
45. T.Y. Fan, R.L. Byer, IEEE J. Quantum Electron. **24**, 895 (1988)
46. W. Koechner, *Solid-state Laser Engineering* (Springer, Heidelberg, 2006)
47. H. Mirzaeian, S. Manjooran, A. Major, SPIE Proc. **9288**, 928802 (2014)
48. T. Waritanant, A. Major, Appl. Phys. B **122**, 135 (2016)
49. T. Waritanant, A. Major, Opt. Express **24**, 12851 (2016)
50. R.C. Talukder, M.Z.E. Halim, T. Waritanant, A. Major, Opt. Lett. **41**, 3810 (2016)
51. M. Nadimi, T. Waritanant, A. Major, Photon. Res. **5**, 346 (2017)
52. M.Z.E. Halim, R.C. Talukder, T. Waritanant, A. Major, Laser Phys. Lett. **13**, 105003 (2016)
53. C.Y. Li, Y. Bo, J.L. Xu, C.Y. Tian, Q.J. Peng, D.F. Cui, Z.Y. Xu, Opt. Commun. **284**, 4574 (2011)
54. X.Z. Wang, Z.F. Wang, Y.K. Bu, L.J. Chen, G.X. Cai, Z.P. Cai, IEEE Photon. J. **6**, 1 (2014)